Particuology 83 (2023) 156–168

Contents lists available at ScienceDirect

Particuology

journal homepage: www.elsevier.com/locate/partic

Study of biomass gasification in an industrial-scale dual circulating fluidized bed (DCFB) using the Eulerian-Lagrangian method

Jiahui Yu [a], Shuai Wang [a], Kun Luo [a, b, *], Debo Li [c], Jianren Fan [a, b]

[a] State Key Laboratory of Clean Energy Utilization, Zhejiang University, Hangzhou, 310027, China
[b] Shanghai Institute for Advanced Study of Zhejiang University, Shanghai, 200120, China
[c] Guangdong Diankeyuan Energy Technology Co., Ltd., Guangzhou, 510080, China

ARTICLE INFO

Article history:
Received 21 December 2022
Received in revised form
17 February 2023
Accepted 26 February 2023
Available online 10 March 2023

Keywords:
Dual fluidized bed
Biomass gasification
Numerical simulation
MP-PIC
Heat transfer coefficient

ABSTRACT

Dual circulating fluidized bed (DCFB) has emerged as an efficient reactor for biomass gasification due to its unique feature of high gas-solid contact efficiency and separated reactions in two reactors, yet the understanding of complex in-furnace phenomena is still lacking. In this study, biomass gasification in an industrial-scale DCFB system was numerically studied using a multiphase particle-in-cell (MP-PIC) method featuring thermochemical sub-models (e.g., heat transfer, heterogeneous reactions, and homogeneous reactions) under the Eulerian-Lagrangian framework. After model validation, the hydrodynamics and thermochemical characteristics (i.e., pressure, temperature, and species) in the DCFB are comprehensively investigated. The results show that size-/density-induced segregation makes solid fuels concentrate on the bed surface. Interphase momentum exchange leads to the continuous decrease of the gas pressure axially. In the gasifier and combustor, the lower heating value (LHV) of the gas products is 5.56 MJ/Nm^3 and 0.2 MJ/Nm^3 and the combustible gas concentration (CGC) is 65.5% and 1.86%, respectively. The temperature in the combustor is about 100 K higher than that in the gasifier. A higher solid concentration results in a smaller value of particle heat transfer coefficient (HTC). The HTCs range from 50 to 150 W/(m^2 K) for a solid concentration larger than 0.3 in the combustor while the HTCs range from 100 to 200 W/(m^2 K) in the gasifier. The Reynolds number of biomass particles is two orders of magnitude larger than that of the sand particle. The numerical results shed light on the reactor design and process optimization of biomass gasification in DCFBs.

1. Introduction

The increasing depletion of fossil energy resources and climate change urge people to seek renewable and sustainable energy as an alternative to the current fossil energy (Ge et al., 2014). Among all clean energy resources, biomass attracts tremendous attention from both academic and engineering communities (Huang et al., 2023). Compared with other treatment methods (i.e., landfill, incineration), biomass gasification is one of the most used technologies because it thermochemically converts the solid carbonaceous feedstock into gaseous products (Gómez-Barea & Leckner, 2010; Rahman et al., 2019), which benefits the downstream synthesis of chemical products (e.g., methanol, ammonia, fertilizer). Due to its good temperature control, excellent gas-solid mixing, and wide fuel flexibility, the fluidized bed reactor is a good choice for biomass gasification (Wang et al., 2023). Fluidized bed reactors have different types, generally including fixed bed (FB), bubbling fluidized bed (BFB), spouting bed (SB), turbulent fluidized bed (TFB), and circulating fluidized bed (CFB). Recently, the combination of these two reactors into a dual fluidized bed (DFB) has been increasingly employed due to the unique feature of separating the nitrogen from the gaseous products in the gasifier, supporting endothermic gasification based on the heat supplied by the combustor, and transporting heat between two reactors by heat carriers (Myöhänen et al., 2018), as shown in Fig. 1. DFB has the advantage of producing syngas with moderate high heating value (HHV) and low tar levels under a wide range of biomass materials. Accordingly, the DFB has emerged to be established worldwide (Kraft et al., 2017; Mauerhofer, Müller, et al., 2019). However, the

* Corresponding author. State Key Laboratory of Clean Energy Utilization, Zhejiang University, Hangzhou, 310027, China.
E-mail address: zjulk@zju.edu.cn (K. Luo).

https://doi.org/10.1016/j.partic.2023.02.018

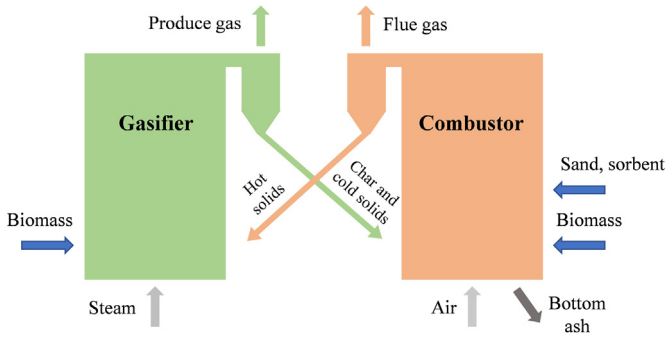

Fig. 1. Schematic of the dual fluidized bed.

complex gas-solid hydrodynamics together with intense thermochemical behaviour in the DFB is far away from being fully understood, which inhibits reactor design and process optimization.

In the past few years, many experiments have been performed to study flow dynamics and biomass gasification in DFBs, involving the substitution of air with CO_2 as a gasifying agent (Mauerhofer, Müller, et al., 2019), assessment of gas quality (Mauerhofer et al., 2019), prediction of tar formation (Benedikt et al., 2019), distribution of solid fraction (Lim et al., 2015), design of new reactors (Kuba et al., 2018). Such experiments provided abundant macro-scale information on biomass gasification in DFBs, benefiting both academic and engineering communities. However, the experimental method faces an intrinsic challenge in unveiling the complex in-furnace phenomena (e.g., solid back-mixing, particle segregation, cluster formation, and non-uniform distribution) due to its intrinsic limitations. Besides, the experiment is time-consuming and limited in a narrow operating window.

With the improvement of computer capacity and numerical algorithms, simulation provides a cost-effective, repeatable, and systematic method to study biomass gasification in fluidized beds (Wang et al., 2020; Wang & Shen, 2022). Based on the treatment method of solid phases, the numerical method can be divided into the Eulerian-Eulerian framework and the Eulerian-Lagrangian framework (Van et al., 2008). The former assumes both gas and solid phases as continuous media, providing a fast solution to describe flow dynamics and biomass gasification in the DFB (Yan et al., 2018). However, this method has the intrinsic limitation in obtaining reasonable information about dispersed particles, such as particle size distribution and particle shrinkage. In contrast, the Eulerian-Lagrangian method tracks the trajectory of each particle and features the inherent information of dispersed particles, thus has emerged as a promising way to simulate dense gas-solid reacting flow (Wang et al., 2023). Under the Eulerian-Lagrangian framework, the computational fluid dynamics — discrete element method (CFD-DEM) fully resolves inter-particle collisions using tiny solid time steps, leading to the unaffordable computational costs in simulating large-scale fluidized bed reactors within enormous particles (Hu et al., 2019; Wang & Shen, 2020). Specifically, the CFD-DEM is commonly applied to simulate biomass gasification in small-scale fluidized bed reactors, with a focus on the fundamental study of particle trajectory (Tsuji et al., 1993), heat transfer contribution (Hou et al., 2012), solid fuel conversion (Kong et al., 2022), bubble dynamics (Yang et al., 2019), and so on. In contrast, the multiphase particle-in-cell (MP-PIC) as another Eulerian-Lagrangian method is more efficient in simulating dense gas-solid reacting flow than the CFD-DEM, as it lumps several original particles with identical properties into a numerical parcel and further simplifies inter-particle collisions with a solid stress model (Snider et al., 2011). These two strategies reduce computational costs tremendously, making the MP-PIC intrinsically applicable for the simulation of large-scale fluidized bed reactors with large amounts of particles. Using this approach, Kong et al. (2020) studied the thermochemical behaviour of gas-solid flow in a pilot-scale DFB composed of a BFB gasifier and a CFB combustor. Yang et al. (2020) investigated the radial and axial segregation of heat carriers in a pilot-scale 1MW_{th} DFB including a BFB gasifier and a CFB gasifier. Based on the same apparatus, Liu et al. (2015) mainly focused on the effects of the particle size distribution (PSD) and drag models on the gasification performance. In summary, the reports about the numerical study of the DFB are very limited due to its complex geometries and intricate chemical reactions. Moreover, the available studies of the DFB are commonly limited to the pilot-scale capacity and the gasifier usually facilitates with a BFB, which hinders the application of the DFB in the practical engineering fields.

Accordingly, an industrial-scale DFB with a new design where the combustor and gasifier operate at the fast fluidization regime is numerically studied by the MP-PIC method featuring thermochemical sub-models. The particle-scale properties and thermochemical characteristics of dense gas-solid reacting flow in the dual circulating fluidized bed (DCFB) are comprehensively studied, with a mechanism elucidation of heat and mass transfer behaviour. The present work is structured as follows: Section 2 details the mathematical model, reaction kinetics, and model validation. Section 3 gives the numerical settings. Typical flow patterns are presented in section 4.1. Section 4.2 presents the pressure and temperature distribution, followed by the gas species contribution in section 4.3. Heat and mass transfer mechanisms are presented in section 4.4. The conclusion is drawn in Section 5.

2. Mathematical model

In this work, the MP-PIC framework featuring thermochemical sub-models was developed to study the biomass gasification process. Specifically, the volume-averaged Navier-Stokes equations are used to describe gas motion. A parcel concept is introduced to reduce the particle number by lumping a collection of particles into a parcel. Reaction kinetics of biomass gasification regarding heterogeneous and homogeneous reactions are implemented. Sand and biomass are assumed as spherical without particle morphology considered, due to the incapability of the MP-PIC method in simulating non-spherical particles (Snider, 2001; Snider et al., 2011). Moreover, it is acceptable to assume the solid fuels (e.g., biomass, coal) as spherical particles in such an industrial-scale fluidized bed apparatus, which has been demonstrated by many previous simulations (Kraft et al., 2017; Snider et al., 2011; Xie et al., 2017). In this section, the MP-PIC framework is first briefly introduced, followed by the description of reaction kinetics regarding biomass gasification.

2.1. MP-PIC framework

The conservation equations for the gas phase involving mass, momentum, energy, and species conservation are given by (Snider et al., 2011):

$$\frac{\partial(\varepsilon_g\rho_g)}{\partial t}+\nabla\cdot(\varepsilon_g\rho_g\boldsymbol{u}_g)=\delta\dot{m}_p \tag{1}$$

$$\frac{\partial(\varepsilon_g\rho_g\boldsymbol{u}_g)}{\partial t}+\nabla\cdot(\varepsilon_g\rho_g\boldsymbol{u}_g\boldsymbol{u}_g)=-\varepsilon_g\nabla p+\varepsilon_g\rho_g\boldsymbol{g}+\nabla\cdot(\varepsilon_g\tau_g)+\boldsymbol{F}_{gp} \tag{2}$$

$$\frac{\partial(\theta_g\rho_g h_g)}{\partial t}+\nabla\cdot(\theta_g\rho_g\boldsymbol{u}_g h_g)=\theta_g\left(\frac{\partial p_g}{\partial t}+\boldsymbol{u}_g\cdot\nabla p_g\right)-\nabla\cdot(\theta_g q)+\dot{Q}_D+S_{gp}-\Delta H_{rg} \tag{3}$$

$$\frac{\partial(\varepsilon_g\rho_g X_i)}{\partial t}+\nabla\cdot(\varepsilon_g\rho_g\boldsymbol{u}_g X_i)=\nabla\cdot(\varepsilon_g\rho_g D_i\nabla X_i)+\delta\dot{m}_{gi}+\delta\dot{m}_{pi} \tag{4}$$

where ε_g, ρ_g, p, and $\boldsymbol{u}_g$ are the voidage, density, pressure, and velocity of the gas phase, respectively. $\delta\dot{m}_p$ is the consumption or generation rate due to heterogeneous reactions. $\boldsymbol{F}_{gp}$ is the interphase momentum exchange term. τ_g is the gas stress tensor. h_g and ΔH_{rg} are the gas enthalpy and heat of reaction, respectively. S_{gp} is the interphase energy exchange term. $\dot{Q}_D$ is the enthalpy diffusion term. X_i is the mass fraction of species i. $\delta\dot{m}_{gi}$ and $\delta\dot{m}_{pi}$ are the consumption or generation rate of species i due to heterogeneous reactions and heterogeneous reactions, respectively. $D_i\,(=\mu_g/\rho_g S_C)$ is the turbulent mass diffusion rate of species i, whereby μ_g is the gas viscosity and Sc is the Schmidt number. The detailed calculation of these items can refer to the previous literature (Snider et al., 2011).

The dynamics of the particle phase are described by solving the particle distribution function (PDF) f as follows (O'Rourke & Snider, 2012):

$$\frac{\partial f}{\partial t}+\frac{\partial(f\boldsymbol{u}_p)}{\partial t}+\frac{\partial(f\mathbf{A})}{\partial\boldsymbol{u}_p}=\frac{f_D-f}{\tau_D}+\frac{f_G-f}{\tau_G} \tag{5}$$

where f_D is the particle distribution function at local equilibrium, and τ_D is the particle collision relaxation time. After the particle collision, the velocity tends to be the isotropic Gaussian distribution, and τ_G and f_G are the relaxation time and particle distribution functions in this state. The particle acceleration **A** is formulated as:

$$\mathbf{A}=\frac{d\boldsymbol{u}_p}{dt}=\beta(\boldsymbol{u}_g-\boldsymbol{u}_p)-\frac{\nabla p}{\rho_p}-\frac{\nabla\tau_p}{\rho_p\varepsilon_p}+\boldsymbol{g}+\frac{\overline{\boldsymbol{u}}_p-\boldsymbol{u}_p}{2\tau_D} \tag{6}$$

where, $\overline{\boldsymbol{u}}_p$ is the local mass average particle velocity. τ_p is the solid normal stress related to particle collisions. The solid volume fraction, interphase momentum exchange term, and interphase energy exchange term are respectively formulated as:

$$\varepsilon_p=\iiint f\frac{m_p}{\rho_p}dm_p d\boldsymbol{u}_p dT_p \tag{7}$$

$$\boldsymbol{F}_{gp}=-\iiint f_s\left\{m_s\left[D_s(\boldsymbol{u}_g-\boldsymbol{u}_p)-\frac{\nabla p_g}{\rho_p}\right]+\boldsymbol{u}_p\frac{dm_p}{dt}\right\}dm_p d\boldsymbol{u}_p dT_{sp} \tag{8}$$

$$S_{gp}=\iiint f_p\left\{m_p\left[D_p(\boldsymbol{u}_g-\boldsymbol{u}_p)^2-C_V\frac{dT_p}{dt}\right]-\frac{dm_p}{dt}\left[h_p+\frac{1}{2}(\boldsymbol{u}_g-\boldsymbol{u}_p)^2\right]\right\}dm_p d\boldsymbol{u}_p dT_p \tag{9}$$

where m_p, $\boldsymbol{u}_p$, and T_p are the mass, velocity, and temperature of the particle phase, respectively. D_s is the drag coefficient, which is calculated using the correlation proposed by Gidaspow (1994). Besides, each particle is assumed to be iso-thermal, indicating the thermal gradient inside the particle is not considered in the current model. The energy conservation for the particle is formulated as:

$$m_p C_V\frac{dT_p}{dt}=Q_{pg}+Q_{radi}-\Delta H_{rp} \tag{10}$$

$$Q_{pg}=\frac{\kappa_g \mathrm{Nu}_p}{d_p}A_p(T_g-T_p) \tag{11}$$

$$Q_{radi}=\sigma\varepsilon_p A_p\left(T_{b,local}^4-T_p^4\right) \tag{12}$$

$$\mathrm{Nu}_p=2.0+0.6\mathrm{Re}_p^{1/2}\,\mathrm{Pr}^{1/3} \tag{13}$$

$$\mathrm{Re}_p=\frac{\rho_g\varepsilon_g|\boldsymbol{u}_g-\boldsymbol{u}_p|d_p}{\mu_g} \tag{14}$$

$$\mathrm{Pr}=\mu_g C_{p,g}\big/\kappa_g \tag{15}$$

where particle Nusselt number Nu_p is calculated by combining the particle Reynolds number Re_p and Prandtl number Pr. A_p, ε_p, and σ are the particle surface area, emissivity, and Stefan-Boltzmann constant, respectively. $T_{b,local}$ is the temperature of the surrounding environment. The detailed calculation of these terms can refer to the previous literature (Snider et al., 2011).

2.2. Reaction kinetics

In the DCFB system, biomass is chosen as the reactive material containing volatile, moisture, char, and ash. When the fuel enters the gasifier and combustor, a variety of chemical reactions take place simultaneously. Fig. 2 shows the reaction model for the thermochemical conversion of a biomass particle. Heterogeneous and homogeneous reactions take place in the reactor. Accordingly, the global reaction kinetics is implemented considering drying, pyrolysis, heterogeneous reactions and homogeneous reactions.

As the temperature increases, the moisture is first evaporated as steam through the drying process, which is denoted by:

$$\text{Moisture in biomass (s)}\rightarrow H_2O\text{ (g)} \tag{R1}$$

The evaporation rate of moisture can be calculated by (Yan et al., 2016):

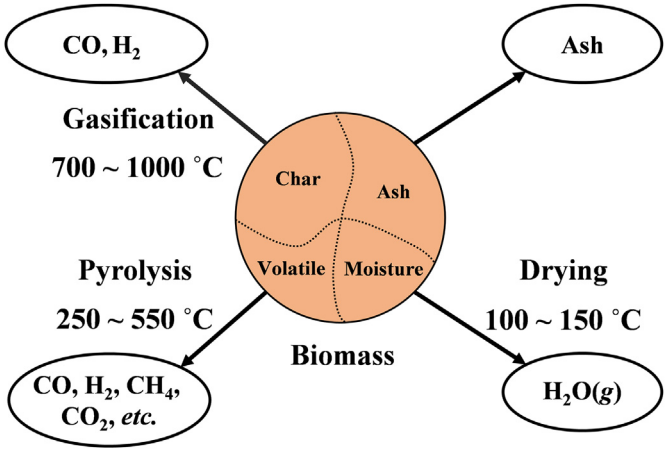

Fig. 2. Schematic of the biomass gasification process.

$$\frac{dm_{moisture}}{dt} = NA_pM_W \tag{16}$$

where A_p is the particle surface area and M_W is the molar weight of the moisture. N is the vapour molar flux and is formulated as:

$$N = k(C_{p,s} - C_{p,\infty}) \tag{17}$$

$$k = \frac{\mathrm{Sh}D}{d_p}; \quad C_{p,s} = \frac{P_{sat,Tp}}{RT_p}; \quad C_{p,\infty} = X_i\frac{P}{RT_\infty} \tag{18}$$

where Sh is the Sherwood number and D is the diffusion coefficient. $P_{sat,Tp}$ and P represent the saturation and local pressure, respectively. X_i is the gaseous species mass fraction.

During the pyrolysis process, many gaseous species (e.g., CO, H_2, CH_4, and CO_2) are released. The pyrolysis process can be given by:

$$\text{Biomass} \rightarrow \alpha_1\mathrm{CO} + \alpha_2\mathrm{CO_2} + \alpha_3\mathrm{H_2} + \alpha_4\mathrm{CH_4} + \alpha_5\mathrm{C_2H_4} + \alpha_6\mathrm{C_2H_6} + \alpha_7\mathrm{Char_{(s)}} + \alpha_8\mathrm{Ash_{(s)}} \tag{R2}$$

where α_i is the mass fraction of i^{th} species and the summation of it is unity. Moreover, the tar formation process is not considered due to its insignificant effect on bed hydrodynamics (Kraft et al., 2017). The pyrolysis rate is given by (Badzioch & Hawksley, 1970):

$$\frac{dm_{volatile}}{dt} = -5 \times 10^6 \exp(-14433 / T_p)m_{volatile} \tag{19}$$

where $m_{volatile}$ is the mass of volatile in the biomass particles.

The char reacts with the surrounding gasifying agents after the pyrolysis process. The process of char conversion is influenced by diffusion and kinetics effects. Thus, the classic model proposed by Baum and Street (1971) is adopted:

$$\frac{dm_{c-i}}{dt} = -A_pp_i\frac{k_{diff,i}k_{kin,i}}{k_{diff,i} + k_{kin,i}} \tag{20}$$

where p_i is the particle pressure. $k_{diff,i}$ and $k_{kin,i}$ are the diffusion and kinetic rate coefficients, respectively.

$$k_{diff,i} = C_i\frac{\left[0.5(T_p + T_g)\right]^{0.75}}{d_s}; \quad k_{kin,i} = A_iT_p\exp\left(-\frac{E_i}{RT_p}\right) \tag{21}$$

where C_i is the model constant, 5.0×10^{-12} s $K^{-0.75}$. A_i is the pre-exponential factor and E_i represents the activation energy. Moreover, homogeneous reactions such as water-gas shift, methane oxidation and hydrogen oxidation are considered in this work. The details of all reactions and their kinetics are listed in Table 1.

2.3. Model validation

As the experimental data of the investigated apparatus are unavailable, the integrated model is first validated with biomass gasification in a three-dimensional (3D) CFB gasifier experimentally conducted by Garíca-Ibañez et al. (2004). Fig. S1(a) presents the schematic of the CFB gasifier (Figs. S1–S5 are in the Supplementary Data). The mean diameter and density of the biomass particles are 1.89 mm and 659 kg/m^3, respectively. The silica sand is chosen as the bed material with a mean diameter and density of 0.5 mm and 2600 kg/m^3, respectively. The analysis and physical properties of biomass are listed in Table S1 (Tables S1 and S2 are in the Supplementary Data). Primary airflow is introduced from the bottom to fluidize the bed material and acts as a gasifying agent. The secondary airflow is injected from a feeding port 2.15 m above the bottom to support reactions. Detailed computational setup can be found in Table S1. As presented in Fig. S1(b), the mole fraction of the main gas components (i.e., CO, CO_2, H_2, CH_4, hydrocarbon components, and N_2) predicted by the integrated model agrees well with that obtained from experimental measurements. The slight discrepancies stem from the impractical implementation of the numerous elementary reactions during biomass gasification.

An additional model validation towards biomass gasification is conducted in a dual fluidized bed gasifier (DFBG) installed at Woodland Biomass Research Center, Woodland, California. As shown in Fig. S2(a), the DFBG consists of a bubbling fluidized gasifier for gasification and a combustor reactor. At the initial time, the solid materials are packed at the bottom of the reactor with an initial height of 2500 mm. The steam is injected from the gasifier bottom to fluidize the bed materials and gasify the biomass materials. Moreover, the propane is introduced into the combustor. The biomass materials are continuously fed from the side of the gasifier. The analysis and physical properties of biomass are listed in Table S2. As illustrated in Fig. S2(b), the mole fraction of the main gas species agrees well with the experimental data. The slight discrepancy is attributed to the simplification of reaction kinetics. Thus, the present MP-PIC model is reasonable to be used to study biomass gasification in the 3D DCFB. Moreover, the numerical accuracy of the integrated model is not affected by operating conditions (e.g., mass flow rate of solid fuels) as the equations or formula governing gas-solid flow dynamics, heat transfer, and chemical reactions are unchanged. Thus, the integrated model is reliable for the simulation of biomass gasification in the DCFB under different operating conditions.

3. Simulation conditions

A 3D dual circulating fluidized bed (DCFB) system is numerically studied in this work. As shown in Fig. 3, the DCFB system consists of a gasifier and a combustor (My H Nen et al., 2018). The height of the system is 15 m, and the diameter of the gasifier and combustor are 1.6 m and 1.4 m respectively. For the gasifier, the steam is introduced from the bottom to fluidize bed materials and serves as a gratifying agent. The feedstock (i.e., biomass) with additional steam is fed through the feeding port at a height of 1.9 m. For the combustor, air is introduced from the bed to fluidize bed materials. The additional air is fed into the gasifier from the nozzle at the height of 1.1 m. At the height of 0.5 m, additional fuel is fed to the combustor to aid combustion. The particle properties adopted in the current simulation are consistent with the values used by Myöhänen et al. (2018), which were originally provided in the corresponding experiment. The biomass material has a density of 659 kg/m^3 and a particle size distribution (PSD) of 0.05 mm–2.5 mm. The bed material is sand, which has a density of 2300 kg/m^3 and a particle size distribution (PSD) of 0.00025 mm–0.25 mm. The cumulative weight of normal distribution is adopted to describe the PSD, given by:

Table 1
Homogeneous and heterogeneous reactions (Gómez-Barea & Leckner, 2010; Snider et al., 2011; Tokmurzin & Adair, 2019).

Heterogeneous reactions		Kinetic parameters
R3	$C + 0.5O_2 \rightarrow CO$	$A_{O_2} = 2.51 \times 10^{-3}$ s/(m K); $E_{O_2} = 7.48 \times 10^{7}$ J/kmol
R4	$C + CO_2 \rightarrow 2CO$	$A_{CO_2} = 3.0 \times 10^{-1}$ s/(m K); $E_{CO_2} = 2.0 \times 10^{8}$ J/kmol
R5	$C + H_2O \rightarrow CO + H_2$	$A_{H_2O} = 2.0 \times 10^{0}$ s/(m K); $E_{H_2O} = 1.96 \times 10^{8}$ J/kmol
Homogeneous reactions		**Kinetic parameters**
R6	$CH_4 + 2O_2 \rightarrow CO_2 + 2H_2O$	$r_6 = 5.16 \times 10^{13} T_g^{-1} \exp(-15636/T_g)[CH_4][O_2]$
R7	$CH_4 + H_2O \rightarrow CO + 3H_2$	$r_7 = 3.0 \times 10^{8} \exp(-15155/T_g)[CH_4][H_2O]$
R8	$H_2 + 0.5O_2 \rightarrow H_2O$	$r_8 = 1.08 \times 10^{12} \exp(-15035/T_g)[H_2][O_2]$
R9	$CO + 0.5O_2 \rightarrow CO_2$	$r_9 = 1.0 \times 10^{10} \exp(-15155/T_g)[CO][O_2]^{0.5}[H_2O]^{0.5}$
R10	$CO + H_2O \leftrightarrow CO_2 + H_2$	$r_{10f} = 2.78 \times 10^{3} \exp(-1515.5/T_g)[CO][H_2O]$
		$r_{10b} = 9.59 \times 10^{4} \exp(-5605/T_g)[CO_2][H_2]$
R11	$C_2H_4 + 3O_2 \rightarrow 2CO_2 + 2H_2O$	$r_{11} = 1.0 \times 10^{12} \exp(-20808/T_g)[C_2H_4][O_2]$
R12	$C_2H_6 + 3.5O_2 \rightarrow 2CO_2 + 3H_2O$	$r_{12} = 4.4 \times 10^{11} \exp(-15199/T_g)[C_2H_6]^{0.5}[O_2]^{1.25}$

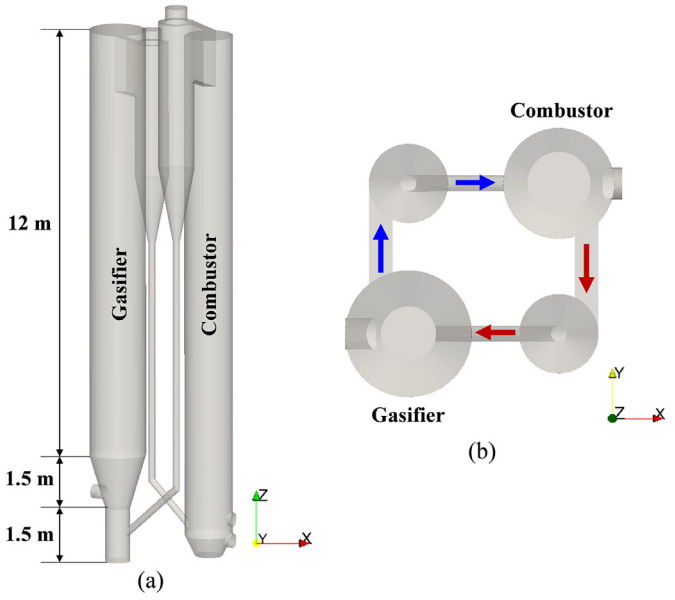

Fig. 3. Geometry and dimensions of the dual circulating fluidized bed (DCFB): (a) front view; (b) top view.

Table 3
Details of operation parameters and boundary conditions.

Parameters	Gasifier	Combustor	Unit
Reactor diameter	1.6	1.4	m
Reactor height	15	15	m
Height of secondary steam	1.9	–	m
Height of secondary air	–	1.1	m
Height of additional duel feed	–	0.5	m
Initial bed temperature	800	880	°C
Steam fed to the gasifier	0.45	–	kg/s
Steam temperature	180	–	°C
Primary steam/air ratio	0.4	–	–
Airflow fed to the combustor	–	1.84	kg/s
Air temperature	–	280	°C
Primary air ratio	–	0.5	–
Fuel fed to the reactor	0.9	0.1	kg/s
Solid fuel temperature	30	30	°C

Table 2
Proximate analysis and ultimate analysis of the biomass (My H Nen et al., 2018).

Proximate analysis, as fired (wt.%)		Ultimate analysis, dry, ash-free (wt.%)	
Fixed carbon	11.1	Carbon	51.0
Volatiles	61.7	Hydrogen	6.1
Moisture	25.0	Nitrogen	0.5
Ash	2.2	Sulphur	0.1
		Oxygen	42.3

$$f = \frac{1}{\sigma\sqrt{2\pi}} e^{-\frac{(d-d_a)^2}{2\sigma^2}} \tag{22}$$

where σ is the standard deviation and d_a is the average particle diameter. The proximate analysis and ultimate analysis of the biomass are summarized in Table 2. Details of the gas-solid parameters and operating conditions are listed in Table 3.

The top of the cyclone is set as a pressure outlet boundary condition. Walls are set as a constant temperature boundary condition. The bottom of the reactor is set as the velocity inlet boundary condition. The whole DCFB system is initially filled with N_2. The simulation is performed for a physical time of 40 s. The computational domain is divided into grids with different resolutions, i.e., coarse grids (85,356), medium grids (171,288), and fine grids (240,560). After the grid-independence test, the results demonstrate that the medium grids are suitable for the subsequent simulations for the sake of balancing numerical accuracy and computational costs. Besides, the number of particles in a parcel (i.e., particle per parcel, $N_{p\text{-}p}$) is crucial for the simulation. $N_{p\text{-}p}$ is specified as 15,625. A larger value of $N_{p\text{-}p}$ corresponds to higher efficiency but lower accuracy while a smaller value of $N_{p\text{-}p}$ corresponds to lower efficiency but higher accuracy. To balance the numerical efficiency and accuracy, $N_{p\text{-}p} = 15{,}625$ is set based on the sensitivity analysis. Three sets of the mass flow rate of solid fuels to the combustor (i.e., 0.05 kg/s, 0.1 kg/s, and 0.15 kg/s) are set to explore their influences on reactor performance.

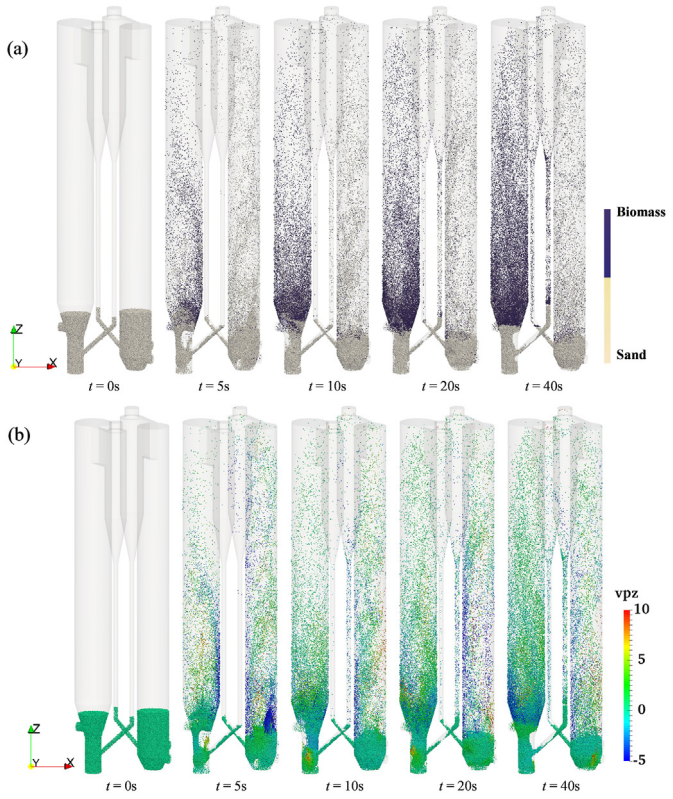

Fig. 4. Flow pattern of particle phase in the dual CFB reactor: (a) solid species; (b) vertical particle velocity (m/s).

4. Results and discussion

4.1. Flow patterns

The flow patterns highly influence the particle mixing, heat transfer, and chemical reactions in the DCFB system, thus they are investigated first. Fig. 4 presents the time-evolution distribution of particle species and vertical velocity in the system. Different flow characteristics of the solid phase can be observed. Particle properties (e.g., size, density) lead to the different fluidization and segregation behaviour in fluidized bed reactors, which has been evidenced in a set of previous experiments and simulations (Chew et al., 2010; Liu & Chen, 2010; Wang et al., 2015; Yang et al., 2021). As shown in Fig. 4(a), sand particles are packed at the lower part of the system initially. Subsequently, biomass particles are fed into the system through the feeding ports of the gasifier and combustor together with the secondary flow. With the introduction of the fluidizing gas, particles move upwards due to the intense momentum exchange with the gas flow. After 5 s, several particles move into the cyclone and then are separated from the gas-solid flow due to the special geometry configuration (Derksen et al., 2008). Gas species are discharged from the separator and particles fall into the riser. Compared with the combustor, more biomass particles exist in the gasifier. Moreover, severe size-induced and density-induced segregation of the solid fuels is observed in the two reactors. Therefore, optimization methods need to be introduced to inhibit the segregation phenomenon and improve the mixing of bed materials (i.e., sand) and solid fuels (i.e., biomass and char). As shown in Fig. 4(b), under the influence of gravity, most particles reaching the maximum heights move downwards along with the periphery of the inner wall, which is termed a solid backmixing phenomenon.

Fig. 5 presents the axial distributions of solid holdup in the combustor and gasifier, respectively. In general, the bed height of the combustor is about 1.5 m while that of the gasifier is about 2.5 m. The relatively dense solid distribution exists in the lower part of the combustor and gasifier due to the weak gas motion. The difference in bed height of the two reactors is attributed to the distinct cross-section areas. Specifically, a smaller cross-section area of the reactor leads to more vigorous movements of particles due to the more significant interphase momentum interactions in a constraint region. Accordingly, the bed height of the gasifier is higher than that of the combustor. The rapid alternation of the solid holdup at 1 m and 2 m of the gasifier is owing to the recycling of particle flow from the loop seal and feeding port, respectively. Comparatively, the dilute solid holdup is captured in the upper part of the reactor due to the density- and size-segregation phenomena.

4.2. Pressure and temperature distributions

Fig. 6 presents the axial distribution of the pressure in the DCFB reactor. Higher pressure is observed in the lower part of the gasifier and combustor due to the heavy bed materials. The fluidization of bed materials makes the pressure rapidly decrease in the axial direction. It is noted that the pressure of the gasifier is higher than that of the combustor, especially in the lower part of the reactor. The reason is that the smaller cross-section of the gasifier constrains the fluidization of particles, which leads to an increase in pressure. Combined with Figs. 3 and 4, higher solid holdup leads to higher pressure in the reactor. In the upper part of the DCFB, the dilute particle flow results in lower pressure.

Fig. 7 presents the particle temperature and axial distributions of gas temperature in the dual CFB system. As shown in the figure, the temperature of gas and particles in the combustor is about 100 K higher than that in the gasifier. In the combustor, most of the

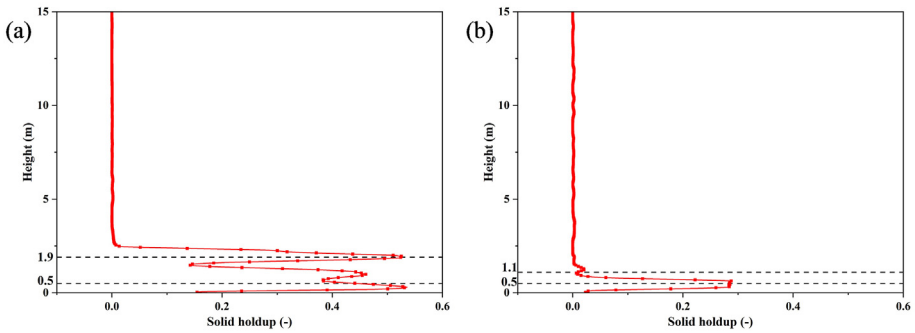

Fig. 5. Axial distributions of solid holdup in the gasifier (a) and combustor (b).

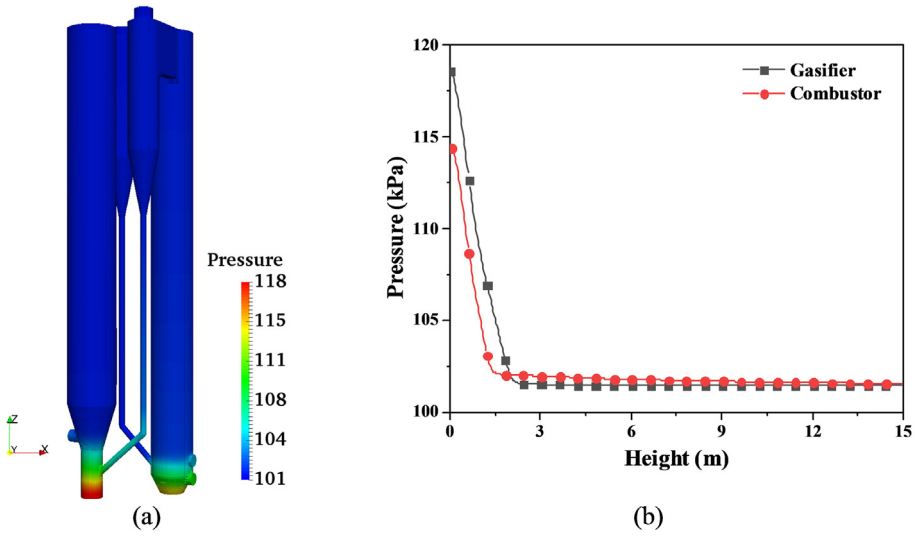

Fig. 6. (a) Contour plot of pressure (kPa) in the DCFB; (b) axial distributions of pressure along the central lines of gasifier and combustor.

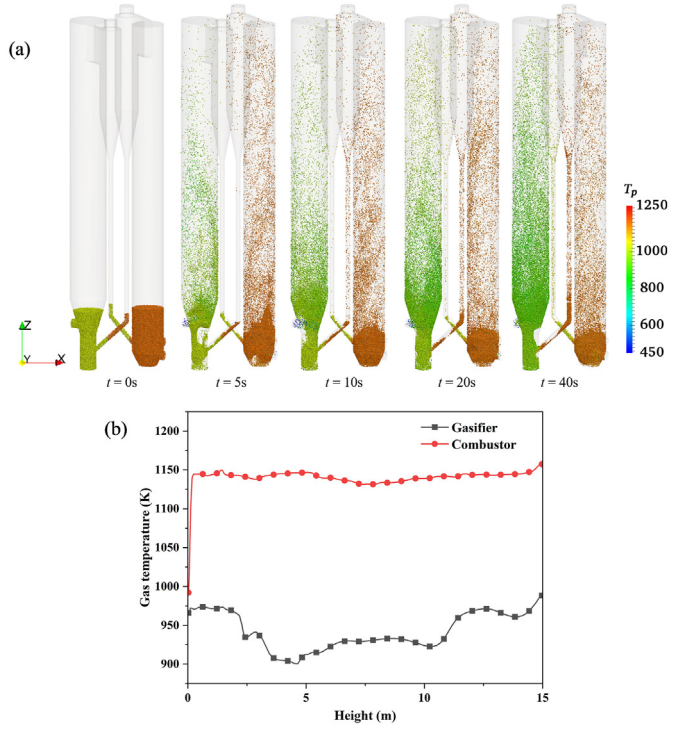

Fig. 7. (a) Contour plot of particle temperature (K) in the dual CFB reactor; (b) axial distributions of gas temperature along the central lines of gasifier and combustor.

fuel burns at the bottom of the combustor with heat released. Thus, the gas temperature at the bottom of the combustor increases sharply while the temperature fluctuation above the height of 1 m is insignificant. In contrast, the gas temperature shows an obvious fluctuation due to the complex chemical reactions in the gasifier. The biomass particles are continuously fed into the gasifier at the height of 1.9 m and undergo the endothermic drying process and devolatilization. Thus, a decrease in gas temperature near the height of 2.5 m can be observed in Fig. 7(b). With the increase in height, the gas temperature increases due to the heat released from exothermic oxidation reactions being stronger than the endothermic reactions.

4.3. Species distribution

Fig. 8 presents the time evolution of gas species mass flow rate released from the outlet of the gasifier and combustor. In the gasifier, the gas species increases because of the volatile release from the introduced biomass particles after the initial period. The mass flow rate of CO_2 is larger than that of CH_4, CO, and H_2. As shown in Figs. S3–S5, the CO_2 and H_2 flow up and gather in the cyclone and upper part of the gasifier at about 20 s, promoting the water-gas-shift reaction ($CO_2 + H_2 \leftrightarrow CO + H_2O$). Thus, the mass flow rate of CO sharply increases at about 22 s with the decrease of the mass flow rate of CO_2. In the combustor, the oxygen reacts with the combustible gases and forms CO_2 while the nitrogen doesn't participate in any reactions. After the initial period, the mass flow rate of N_2 is flatulating around the value of 1.3 kg/s while the mass flow rate of O_2 and CO_2 is around 0.4 kg/s and 0.1 kg/s, respectively. According to the fluctuations of the mass flow rates, it is reasonable to average the concentration of gas species in the last 15 s. Although the concentrations of CO and H_2 in the gasifier fluctuate in the last 15 s, the gas species in the combustor is in a dynamic steady state, which means the heat transferred from the combustor to the gasifier is stable. The industrial-scale dual CFB reactor investigated in this work is very large and requires remarkable computational resources. According to the evidence, many numerical studies of such industrial-scale fluidized bed apparatuses in the open literature were conducted with a physical time of about 30 s (Kong et al., 2020; Xie et al., 2017; Yang et al., 2021). Thus, the physical time of 40 s is suitable for the data analysis of the dual CFB reactor in the following sections.

Fig. 9 presents the distributions of gas species in the dual CFB reactor. The combustible gas species (e.g., C_2H_4, CH_4, H_2, CO) mainly distribute in the gasifier. Fig. 10 numerically presents the axial gas species distributions in the gasifier and combustor, respectively. In the gasifier, the biomass particles are injected into the reactor at a height of 1.9 m and fluidized upwards with the gas phase. The H_2O has a concentration of nearly 100% at the bottom of the gasifier due to the steam being chosen as the fluidization gas. In the lower part of the gasifier, the H_2O sharply decreases its concentration because of the dilution of other gas species produced by devolatilization and gasification of char. The H_2O decreases due to the reaction consumption. Meanwhile, the composition of combustible gas species, such as CO and H_2, is mainly influenced by devolatilization, water-

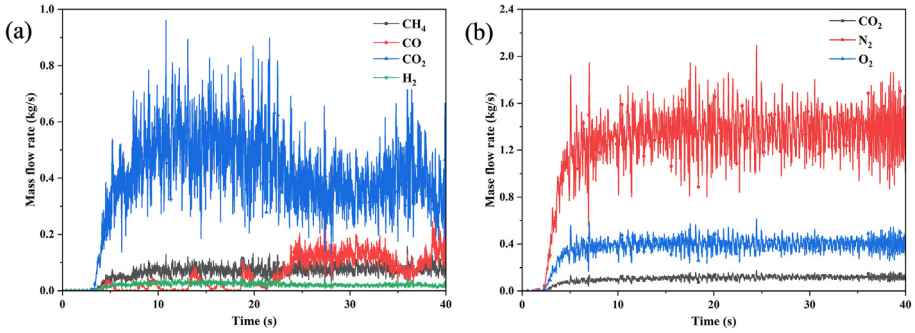

Fig. 8. Time evolution of gas mass flow rate released from the outlet of the gasifier (a) and combustor (b).

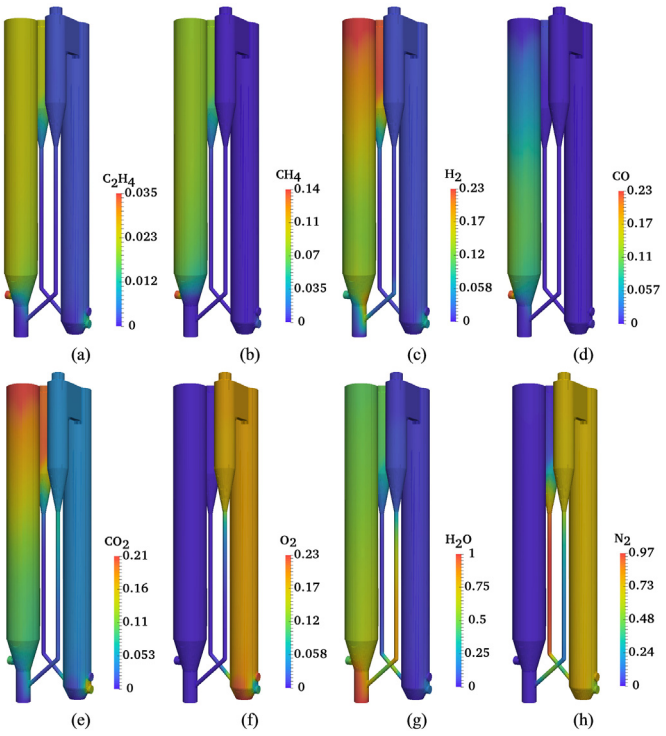

Fig. 9. Contour plots of gas species in the dual CFB reactor: (a) C_2H_4; (b) CH_4; (c) H_2; (d) CO; (e) CO_2; (f) O_2; (g) H_2O; (h) N_2.

concentration while the H_2 increases its concentration because of the shift conversion. As the main reaction product, the concentration of CO_2 increases in the gasifier with the increase in height. In the combustor, most of the biomass particles burn at the lower part and consume O_2. Some combustible gases, such as CH_4 and H_2, can be found near the fuel inlet, but in tiny concentrations. The unique design of the DCFB separates the reactions in two reactors, thus N_2 is focused on the combustor and no N_2 is observed in the gasifier, which demonstrates one of the advantages of the DFB system for biomass gasification.

Figs. 11 and 12 show the distributions of the time-averaged concentrations of gas species (i.e., CO_2 and CO) at different heights (i.e., 0.5 m, 1.0 m, and 2.0 m) in the lower parts of the gasifier. It can be observed that the concentrations of CO_2 and CO in the Y-line are high in the central region. Along with the X-line, the concentrations of CO_2 and CO are high in the right-wall region at the height of 0.5 m and 1.0 m. Especially, at the height of 2.0 m, the concentration of CO_2 first decreases and then increases, while the concentration of CO is large in the near-wall region. Figs. 13 and 14 show the distributions of the time-averaged concentrations of gas species (i.e., CO_2 and O_2) at different heights (h = 0.5 m, 1.0 m, and 2.0 m) in the lower parts of the combustor. The concentration of CO_2 is high in the near-wall region while that of O_2 is small in the near-wall region.

Fig. 15 presents the mean mole fraction of the main combustible gas species (e.g., C_2H_4, CH_4, H_2, CO) at the outlet of the gasifier and combustor under three different mass flow rates of solid fuels fed to the combustor. The change in mass flow rate influences the combustion process in the combustor. As the increase of mass flow rate

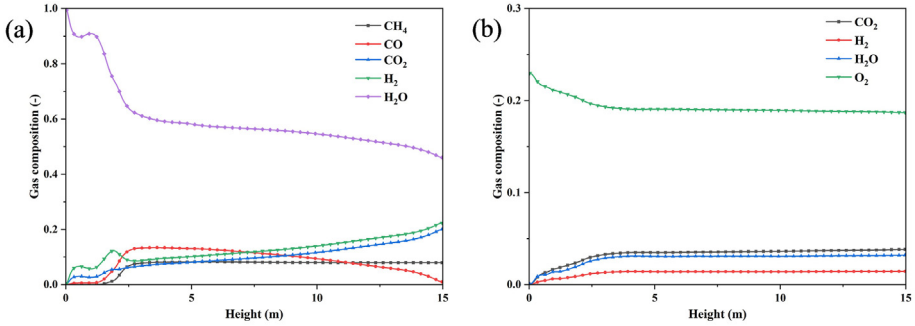

Fig. 10. Main gas composition in the dual CFB reactor: (a) gasifier; (b) combustor.

gas reaction, and shift conversion. As shown in Figs. 9 and 10, the concentrations of CO, CH_4, and H_2 increase in the lower part of the gasifier. In the upper part of the gasifier, the CO decreases its

of solid fuels to the combustor, the concentration of CO_2 increases with the decrease of H_2. In the gasifier, the mean mole fractions of H_2 and CO_2 first decrease and then increase and show the minimum

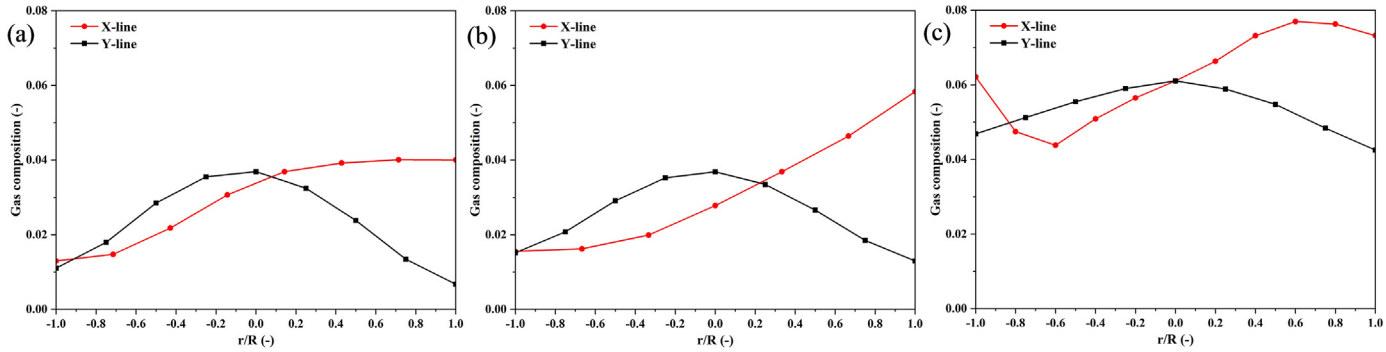

Fig. 11. Distributions of CO_2 concentration at three different heights in the gasifier; (a) h = 0.5 m, (b) h = 1.0 m, (c) h = 2.0 m.

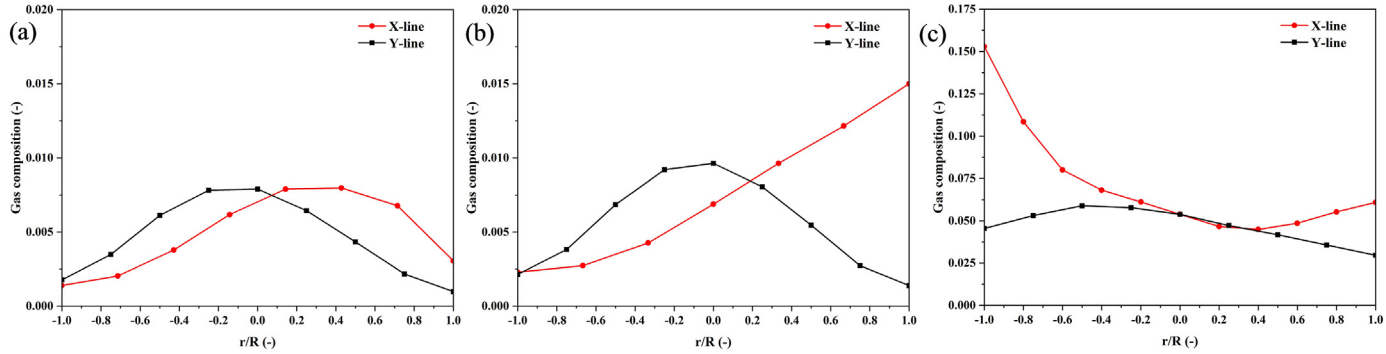

Fig. 12. Distributions of CO concentration at three different heights in the gasifier; (a) h = 0.5 m, (b) h = 1.0 m, (c) h = 2.0 m.

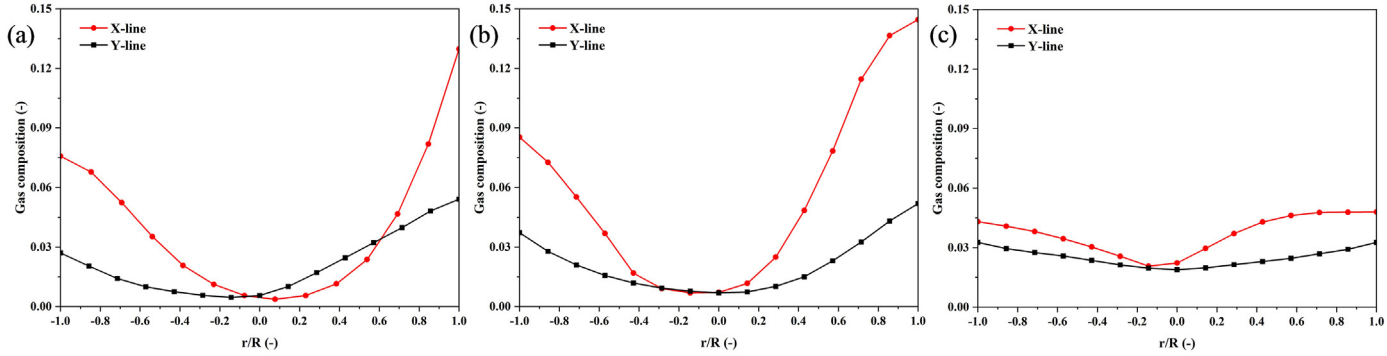

Fig. 13. Distributions of CO_2 concentration at three different heights in the combustor; (a) h = 0.5 m, (b) h = 1.0 m, (c) h = 2.0 m.

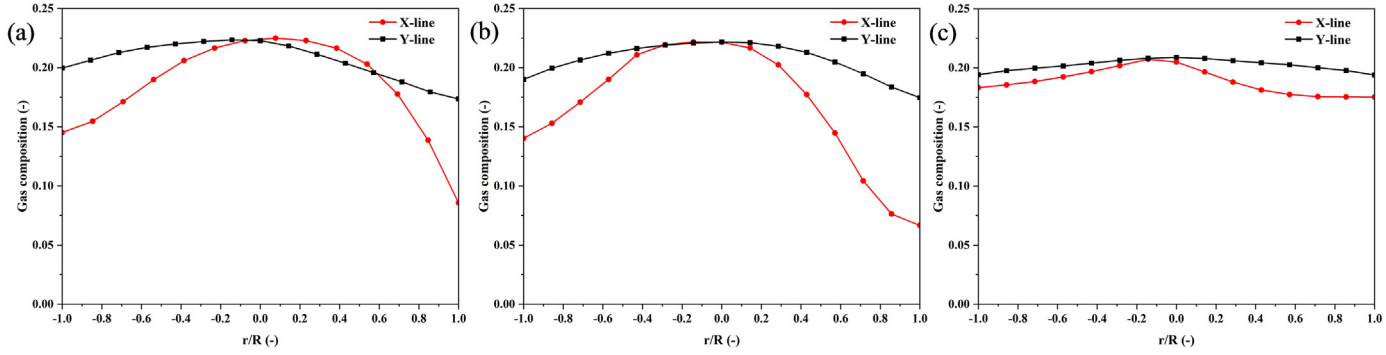

Fig. 14. Distributions of O_2 concentration at three different heights in the gasifier; (a) h = 0.5 m, (b) h = 1.0 m, (c) h = 2.0 m.

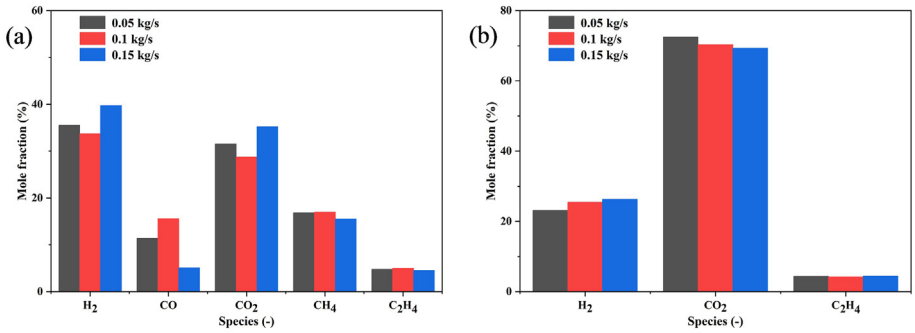

Fig. 15. The effect of the mass flow rate of solid fuels to the combustor on gas composition; (a) gasifier, (b) combustor.

values at the mass flow rate of solid fuels to the combustor of 0.1 kg/s, while the mean mole fractions of CO, CH_4, and C_2H_4 first increase and then decrease and show the maximum values at the mass flow rate of solid fuels to the combustor of 0.1 kg/s.

Two key performance indicators, lower heating value (LHV) and combustible gas (i.e., H_2, CO, CH_4) concentration (CGC), are adopted to evaluate the gasification performance. The LHV and CGC are defined by (Loha et al., 2014):

$$\text{LHV (MJ/Nm}^3) = (25.7 \times H_2\% + 30.3 \times \text{CO}\% + 85.4 \times CH_4\%) \times (\text{February 4, 1000}) \quad (23)$$

$$\text{CGC (\%)} = \text{The volume summation of combustible gas in syngas/Total volume of syngas (without } H_2O) \times 100\% \quad (24)$$

As shown in Fig. 16, in the gasifier and combustor, the LHV of the gas products are 5.56 MJ/Nm^3 and 0.2 MJ/Nm^3, respectively, and the CGC is 65.5% and 1.86%, respectively. In the DCFB system, the biomass gasification process is mainly carried out in the gasifier. Fig. 17 presents the effect of the mass flow rate of solid fuels to the combustor on gasification performance (i.e., LHV and CGC). The change in mass flow rate has a significant influence on the gasification performance of the combustor. With the increase of mass flow rate of solid fuels to the combustor, the value of LHV and CGC increases, which indicates a positive influence on gasification performance. In contrast, for the gasifier, the values of LHV and CGC first increase and then decrease and show the maximum values at the mass flow rate of solid fuels to the combustor of 0.1 kg/s.

4.4. Heat and mass transfer mechanisms

In the CFB reactor, the strong heterogeneous gas-solid flow structures in the fast fluidization regime can significantly influence the solid heat and mass transfer. The heat transfer coefficient (HTC) can be used to characterize gas-solid heat transfer characteristics. The HTC considered for a specific particle with the surrounding environment consists of the convective heat exchange with the gas phase and the radiative heat exchange with the surrounding environment. The HTC of a specific particle is evaluated as (Yang et al., 2021; Zhou et al., 2009):

$$h_s = \left(Q_{pg} + Q_{radi}\right) / A_p \left(T_b - T_p\right) \quad (25)$$

where Q_{pg} and Q_{radi} are the convective heat transfer with the gas phase and the radiative heat exchange with the surrounding environment, evaluated from Eqs. (11) and (12), respectively. Fig. 18 illustrates the relationship of the HTC versus the solid concentration and slip velocity in the combustor. According to Eq. (25), the HTC has a close relationship with the particle Reynolds number, which further correlates with the solid holdup and slip velocity. Accordingly, HTC varies with the change of solid holdup and slip velocity. Specifically, a higher solid concentration results in a smaller value of particle HTC. The HTC ranges from 50 to 150 W/(m^2 K) for a solid concentration larger than 0.3. In contrast, for the dilute distribution of the solid phase, the HTC can reach 400 W/(m^2 K). However, as shown in Fig. 18(b), the HTC of particles ranges from 50 to 150 W/(m^2 K) with a slip velocity smaller than 1 m/s. The dense distribution of the solid phase weakens the motion of the gas phase and also reduces the slip velocity. A larger slip velocity increases the HTC and enhances the heat transfer between the solid and gas phases. For the gasifier, a similar trend can be observed in Fig. 19. The HTC for most particles ranges from 100 to 200 W/(m^2 K), larger than that of the combustor. Thus, the heat transfer characteristics in the gasifier are stronger than that in the combustor.

Figs. 20 and 21 illustrate the variation of the particle temperature (a), HTC (b), slip velocity (c), and Reynolds number (d) of the biomass and sand particles in the combustor and the gasifier, respectively. In the combustor and gasifier, the temperature of sand

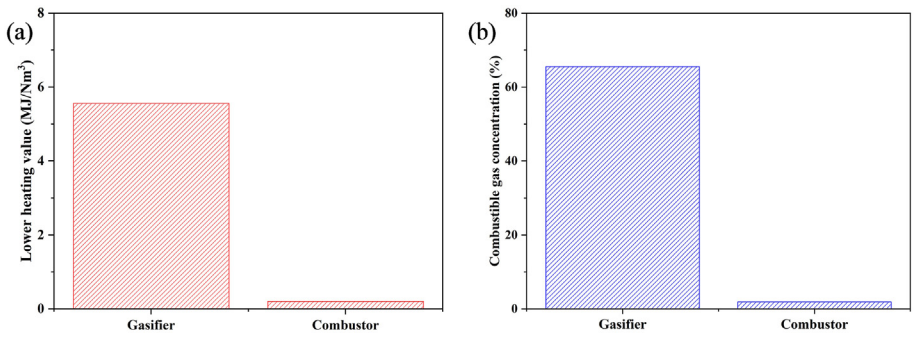

Fig. 16. Comparison of Lower heating value (LHV) (a) and combustible gas concentration (CGC) (b) in the gasifier and combustor.

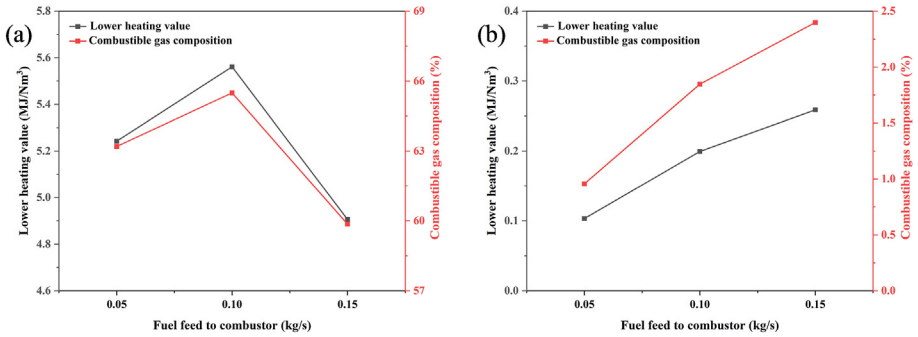

Fig. 17. The effect of the mass flow rate of solid fuels to the combustor on gasification performance (lower heating value and combustible gas concentration); (a) gasifier, (b) combustor.

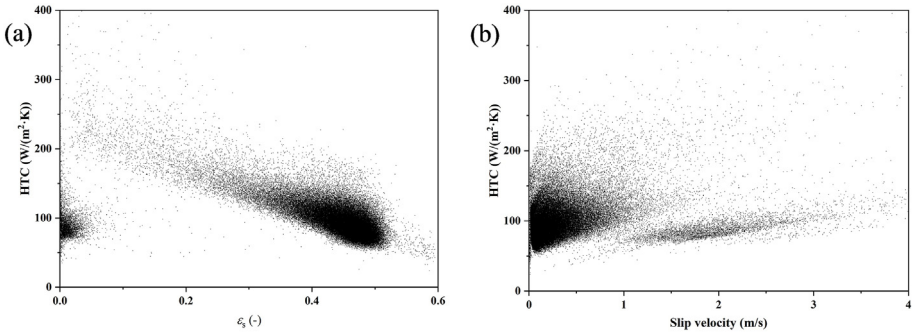

Fig. 18. Relationship of the HTC versus the solid concentration (a) and the slip velocity (b) in the combustor.

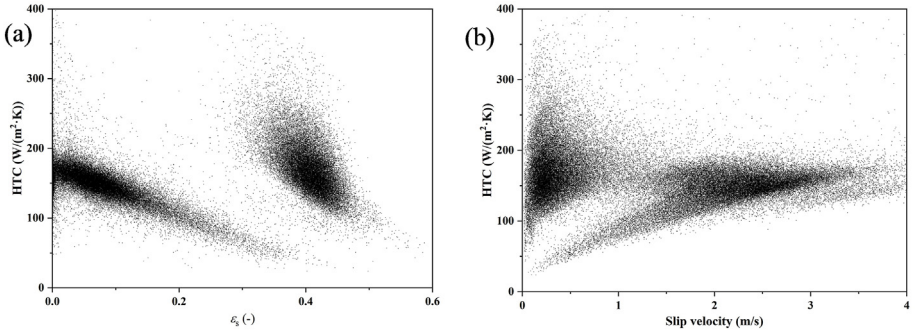

Fig. 19. Relationship of the HTC versus the solid concentration (a) and the slip velocity (b) in the gasifier.

particles keeps nearly constant. For the biomass particles, the temperature increases at the initial time because of the heat exchange with the surrounding environment. After 10 s, the temperature of biomass particles stays constant, showing a good temperature distribution in the DCFB system. The mean biomass particle temperature in the combustor is about 100 K higher than that of the gasifier. The HTCs of biomass and sand particles have similar values in the combustor while the HTC of biomass particles is larger than that of the sand particles in the gasifier. The distribution of the slip velocity and Reynolds number fluctuate around a constant value for both particle species. Compared with the sand particles, the biomass particles have larger slip velocities both in the gasifier and combustor. Especially for the Reynolds number, the value of biomass particles is two orders of magnitude larger than that of the sand particle.

5. Conclusion

In this work, biomass gasification in an industrial-scale DCFB system is numerically studied using the MP-PIC method featuring thermochemical sub-models based on the Eulerian-Lagrangian framework. The integrated model is confirmed to be reliable and reasonable in modelling biomass gasification in fluidized bed reactors. Then, the hydrodynamics and thermochemical characteristics (i.e., pressure, temperature, and species) in the DCFB are comprehensively explored. Conclusions are drawn as follows:

(1) Severe size-induced and density-induced segregation of the solid fuels is observed in the two reactors. Solid back-mixing makes most particles move downwards along with the periphery of the inner wall under the influence of gravity. The bed expansion height of the combustor is about 1.5 m while

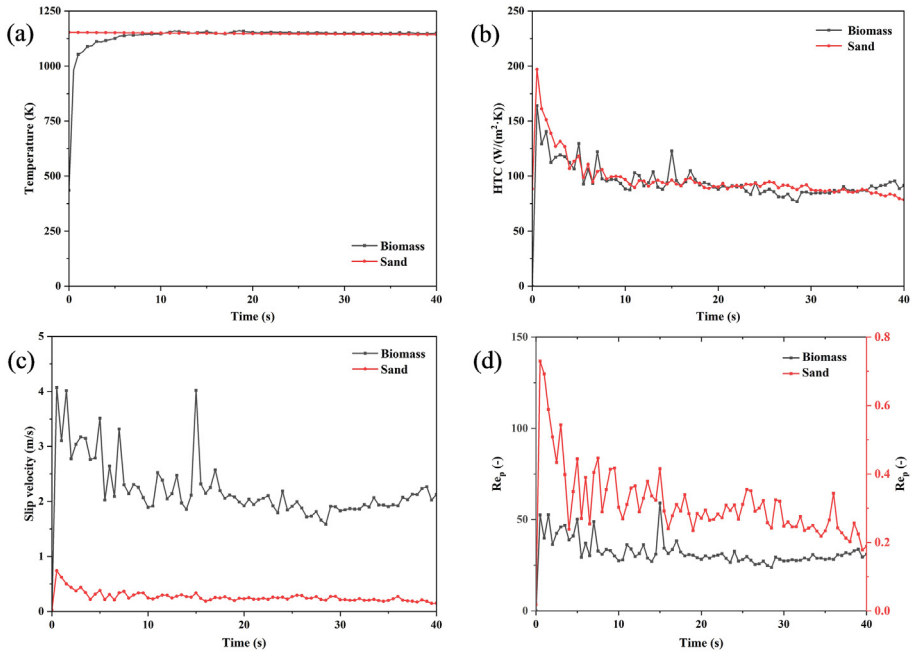

Fig. 20. The variation of the particle temperature (a), HTC (b), slip velocity (c), and Reynolds number (d) of the biomass and sand particles in the combustor.

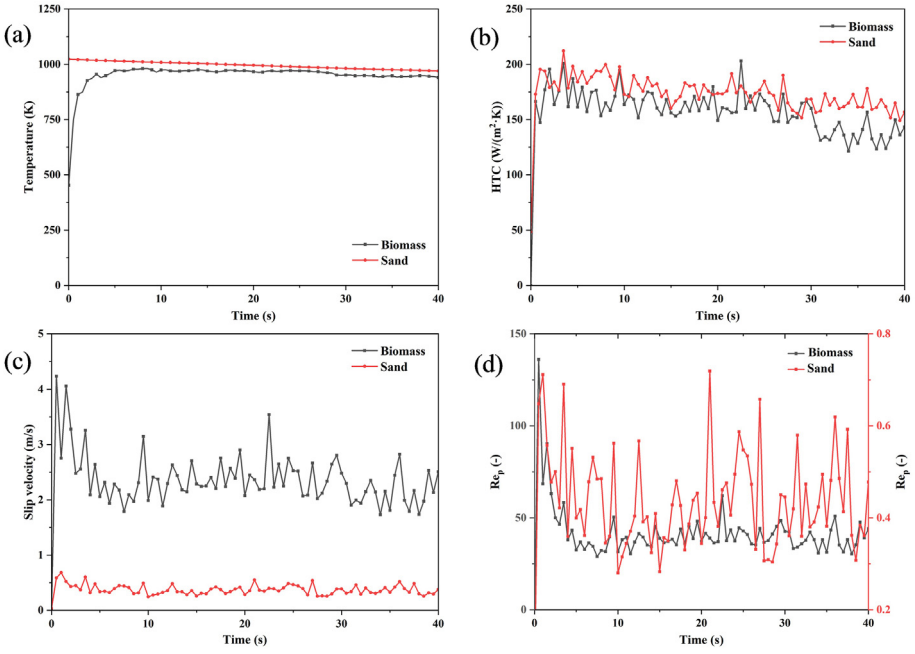

Fig. 21. The variation of the particle temperature (a), HTC (b), slip velocity (c), and Reynolds number (d) of the biomass and sand particles in the gasifier.

that of the gasifier is about 2.5 m. Higher pressure is observed in the lower part of the reactors due to the heavy bed materials and the pressure of the gasifier is higher than that of the combustor. Interphase momentum exchange leads to the continuous decrease of the gas pressure axially.

(2) The combustible gas species are significantly affected by devolatilization, water-gas reaction, and shift conversion. In the upper part of the gasifier, the CO concentration decreases while the H_2 concentration increases due to the shift conversion. As the increase of mass flow rate of solid fuels to the combustor, the CO_2 concentration increases with the decrease of H_2. In the gasifier, the mean mole fractions of H_2 and CO_2 first decrease and then increase and show the minimum values at the mass flow rate of solid fuels to the combustor of 0.1 kg/s, while the mean mole fractions of CO and CH_4 first increase and then decrease and show the maximum values at the mass flow rate of solid fuels to the combustor of 0.1 kg/s. In the gasifier and combustor, the LHV of the gas products is respectively 5.56 MJ/Nm^3 and 0.2 MJ/Nm^3 and the CGC is respectively 65.5% and 1.86%. With the increase of mass flow rate of solid fuels to the combustor, the

values of LHV and CGC increase, indicating a positive influence on the gasification performance in the combustor.

(3) A higher solid concentration results in a smaller value of particle HTC. The HTCs of most particles range from 50 to 150 W/(m^2 K) for a solid concentration larger than 0.3 in the combustor while the HTCs of most particles range from 100 to 200 W/(m^2 K) in the gasifier. The temperature of sand particles keeps nearly constant after the steady state, indicating good temperature control. The temperature of the combustor is about 100 K higher than in the gasifier. A larger slip velocity increases the HTC and accordingly enhances the interphase heat transfer. The Reynolds number of biomass particles is two orders of magnitude larger than that of the sand particle.

The numerical results in this study are helpful for better understanding of hydrodynamics and thermochemical characteristics of biomass gasification in the DCFB.

Declaration of competing interest

The authors declare that they have no known competing financial interests or personal relationships that could have appeared to influence the work reported in this paper.

Acknowledgements

We are grateful for the support from the National Natural Science Foundation of China (grant No. 51925603) and the Fundamental Research Funds for the Central Universities (grant No. 2022ZFJH004).

Appendix A. Supplementary data

Supplementary data to this article can be found online at https://doi.org/10.1016/j.partic.2023.02.018.

References

Badzioch, S., & Hawksley, P. (1970). Kinetics of thermal decomposition of pulverized coal particles. *Industrial and Engineering Chemistry Process Design and Development, 9*(4), 521–530.

Baum, M. M., & Street, P. J. (1971). Predicting the combustion behaviour of coal particles. *Combustion Science and Technology, 3*(5), 231–243.

Benedikt, F., Kuba, M., Schmid, J. C., et al. (2019). Assessment of correlations between tar and product gas composition in dual fluidized bed steam gasification for online tar prediction. *Applied Energy, 238*, 1138–1149.

Chew, J. W., Wolz, J. R., & Hrenya, C. M. (2010). Axial segregation in bubbling gas-fluidized beds with Gaussian and lognormal distributions of Geldart Group B particles. *AIChE Journal, 56*(12), 3049–3061.

Derksen, J. J., Van den Akker, H., & Sundaresan, S. (2008). Two-way coupled large-eddy simulations of the gas-solid flow in cyclone separators. *AIChE Journal, 54*(4), 872–885.

Garíca-Ibañez, P., Cabanillas, A., & Sánchez, J. M. (2004). Gasification of leached orujillo (olive oil waste) in a pilot plant circulating fluidized bed reactor. *Biomass and Bioenergy, 27*, 183–194.

Ge, Z., Li, Y., Li, D., et al. (2014). Thermal energy storage: Challenges and the role of particle technology. *Particuology, 15*, 2–8.

Gidaspow, D. (1994). *Multiphase flow and fluidization: Continuum and kinetic theory descriptions*. Academic press.

Gómez-Barea, A., & Leckner, B. (2010). Modeling of biomass gasification in fluidized bed. *Progress in Energy and Combustion Science, 36*(4), 444–509.

Hou, Q. F., Zhou, Z. Y., & Yu, A. B. (2012). Computational study of heat transfer in a bubbling fluidized bed with a horizontal tube. *AIChE Journal, 58*(5), 1422–1434.

Huang, H., Gao, Y., Chen, H., et al. (2023). Biomass briquette fuel, boiler types and pollutant emissions of industrial biomass boiler: A review. *Particuology, 77*, 79–90.

Hu, C., Luo, K., Wang, S., et al. (2019). Influences of operating parameters on the fluidized bed coal gasification process: A coarse-grained CFD-DEM study. *Chemical Engineering Science, 195*, 693–706.

Kong, D., Luo, K., Wang, S., et al. (2022). Particle behaviours of biomass gasification in a bubbling fluidized bed. *Chemical Engineering Journal, 428*, Article 131847.

Kong, D., Wang, S., Luo, K., et al. (2020). Three-dimensional simulation of biomass gasification in a full-loop pilot-scale dual fluidized bed with complex geometric structure. *Renewable Energy, 157*, 466–481.

Kraft, S., Kirnbauer, F., & Hofbauer, H. (2017). CPFD simulations of an industrial-sized dual fluidized bed steam gasification system of biomass with 8 MW fuel input. *Applied Energy, 190*, 408–420.

Kuba, M., Kraft, S., Kirnbauer, F., et al. (2018). Influence of controlled handling of solid inorganic materials and design changes on the product gas quality in dual fluid bed gasification of woody biomass. *Applied Energy, 210*, 230–240.

Lim, M. T., Saw, W., & Pang, S. (2015). Effect of fluidizing velocity on gas bypass and solid fraction in a dual fluidized bed gasifier and a cold model. *Particuology, 18*, 58–65.

Liu, H., Cattolica, R. J., Seiser, R., et al. (2015). Three-dimensional full-loop simulation of a dual fluidized-bed biomass gasifier. *Applied Energy, 160*, 489–501.

Liu, D., & Chen, X. (2010). Lateral solids dispersion coefficient in large-scale fluidized beds. *Combustion and Flame, 157*(11), 2116–2124.

Loha, C., Chattopadhyay, H., & Chatterjee, P. K. (2014). Three dimensional kinetic modeling of fluidized bed biomass gasification. *Chemical Engineering Science, 109*(16), 53–64.

Mauerhofer, A. M., Müller, S., Benedikt, F., et al. (2019). CO_2 gasification of biogenic fuels in a dual fluidized bed reactor system. *Biomass Conversion and Biorefinery, 11*, 1101–1116.

Mauerhofer, A. M., Schmid, J. C., Benedikt, F., et al. (2019). Dual fluidized bed steam gasification: Change of product gas quality along the reactor height. *Energy, 173*, 1256–1272.

My H Nen, K., Palonen, J., & Hypp Nen, T. (2018). Modelling of indirect steam gasification in circulating fluidized bed reactors. *Fuel Processing Technology, 171*, 10–19.

Myöhänen, K., Palonen, J., & Hyppänen, T. (2018). Modelling of indirect steam gasification in circulating fluidized bed reactors. *Fuel Processing Technology, 171*, 10–19.

O'Rourke, P. J., & Snider, D. M. (2012). Inclusion of collisional return-to-isotropy in the MP-PIC method. *Chemical Engineering Science, 80*(10), 39–54.

Rahman, M. H., Daniel, L., Shah, U., et al. (2019). Estimation of solids circulation rate and char transfer rate from gasifier to combustor in a dual fluidized-bed pilot plant for biomass steam gasification. *Particuology, 46*, 22–29.

Snider, D. M. (2001). An incompressible three-dimensional multiphase particle-in-cell model for dense particle flows. *Journal of Computational Physics, 170*(2), 523–549.

Snider, D. M., Clark, S. M., & O'Rourke, P. J. (2011). Eulerian–Lagrangian method for three-dimensional thermal reacting flow with application to coal gasifiers. *Chemical Engineering Science, 66*(6), 1285–1295.

Tokmurzin, D., & Adair, D. (2019). Development of euler-Lagrangian simulation of a circulating fluidized bed reactor for coal gasification. *Eurasian Chemico-Technological Journal, 21*(1), 45–49.

Tsuji, Y., Kawaguchi, T., & Tanaka, T. (1993). Discrete particle simulation of two-dimensional fluidized bed. *Powder Technology, 77*(1), 79–87.

Van, D., Van, S., Deen, N. G., et al. (2008). Numerical simulation of dense gas-solid fluidized beds: A multiscale modeling strategy. *Annual Review of Fluid Mechanics, 40*(1), 47–70.

Wang, Q., Feng, Y., Lu, J., et al. (2015). Numerical study of particle segregation in a coal beneficiation fluidized bed by a TFM–DEM hybrid model: Influence of coal particle size and density. *Chemical Engineering Journal, 260*, 240–257.

Wang, S., Hu, C., Luo, K., Yu, J., & Fan, J. (2023). Multi-scale numerical simulation of fluidized beds: Model applicability assessment. *Particuology, 80*, 11–41.

Wang, S., Luo, K., & Fan, J. (2020). CFD-DEM coupled with thermochemical sub-models for biomass gasification: Validation and sensitivity analysis. *Chemical Engineering Science, 217*, Article 115550.

Wang, S., & Shen, Y. (2020). CFD-DEM study of biomass gasification in a fluidized bed reactor: Effects of key operating parameters. *Renewable Energy, 159*, 1146–1164.

Wang, S., & Shen, Y. (2022). Coarse-grained CFD-DEM modelling of dense gas-solid reacting flow. *International Journal of Heat and Mass Transfer, 184*, Article 122302.

Xie, J., Zhong, W., Shao, Y., et al. (2017). Simulation of combustion of municipal solid waste and coal in an industrial-scale circulating fluidized bed boiler. *Energy and Fuels, 31*(12), 14248–14261.

Yan, L., Cao, Y., Zhou, H., et al. (2018). Investigation on biomass steam gasification in a dual fluidized bed reactor with the granular kinetic theory. *Bioresource Technology, 269*, 384–392.

Yang, S., Liang, J., Wang, S., et al. (2021). High-fidelity investigation of thermochemical conversion of biomass material in a full-loop circulating fluidized bed gasifier. *Energy, 224*, Article 120093.

Yang, S., Wang, H., Wei, Y., et al. (2019). Numerical investigation of bubble dynamics during biomass gasification in a bubbling fluidized bed. *ACS Sustainable Chemistry & Engineering, 7*(14), 12288–12303.

Yang, S., Wan, Z., Wang, S., et al. (2020). Computational fluid study of radial and axial segregation characteristics in a dual fluidized bed reactor system. *Energy, 209*, Article 118359.

Yan, L., Lim, C. J., Yue, G., et al. (2016). Simulation of biomass-steam gasification in fluidized bed reactors: Model setup, comparisons and preliminary predictions. *Bioresource Technology, 221*, 625–635.

Zhou, Z., Yu, A. B., & Zulli, P. (2009). Particle scale study of heat transfer in packed and bubbling fluidized beds. *AIChE Journal, 55*(4), 868–884.